Wideband 3-D Characterization of Mobile Radio Channels in Urban Environment

Juha Laurila (*Member*), Kimmo Kalliola,
Martin Toeltsch (*Student Member*), Klaus Hugl (*Student Member*),
Pertti Vainikainen (*Member*), and Ernst Bonek (*Senior Member*)

Abstract

This paper describes 3-D radio channel measurements at the base which combines an RF switched receiver array and a synthetic aperture technique and allows full 3-D characterization of the channel. Additionally, dual-polarized patch antennas as array elements enable full determination of the polarization properties of the impinging signals. We describe measurements at over 70 different transmitter positions and three receiver array sites with different sectors and antenna heights. Our results show that the received energy is concentrated within identifiable clusters in the azimuth-elevation-delay domain. We demonstrate that the observed propagation mechanisms are mainly determined by the environment close to the base station. Street canyon propagation dominates also when the receiver array is at or even above rooftop level with the studied measurement distances. Thus the azimuth spectrum at the BS site is fairly independent of the location of the mobile. Signal components propagating over the rooftop are often related to reflections from high-rise buildings in the surroundings.

Keywords

Mobile Radio Channel, Channel Sounding, Spatial Channel Modeling, Adaptive Antennas, DOA Estimation

I. Introduction

Adaptive antennas for second and third generation mobile communication systems have raised significant interest during the last years [1]. Realistic channel models are a prerequisite for performance evaluation of different adaptive antenna solutions and the estimation of the obtainable capacity gain. An introduction to different modeling approaches is given in [2]. Another overview article [3] considers different measurement techniques and contains an extensive literature list. Realistic models require channel measurements to prove their assumptions and to enable appropriate parameter selection.

This paper describes dual-polarized wideband spatial channel measurements at the base station (BS) site in an urban environment. We apply a technique that resolves the direction of arrival (DOA) of the incoming waves both in azimuth and elevation with a delay resolution of $33\,ns$ (full 3-D characterization). Previous characterizations of the mobile radio channel have focused on azimuth and delay only [4] and [5]. Dual-polarized measurements with a four-element array were described in [6]. Our measurement scheme combines RF-multiplexing over the physical array with a synthetic aperture technique, which constructs a virtual planar array structure. The total size of the synthetic aperture was 16×58 elements ($8 \times 29\lambda$). Our physical array consisted of 16 dual-polarized patch elements in order to characterize the polarization of the incoming waves completely.

Wideband 3-D measurements have been performed previously at the mobile station (MS) site at street level [7], [8], [9]. Spatial uplink measurements at the base station (BS) site are especially interesting because first commercial adaptive antenna systems will be located at the BS.

The main goal of this paper is to improve understanding of the urban propagation mechanisms and provide information for channel modeling purposes, in particular by addressing the following questions: Which environments lead to street canyon dominated propagation? Are there single or multiple DOAs dominating the azimuthal delay power spectrum (ADPS)? What is the relative importance of near-by or far-reflected components? Do the signal components that are diffracted over the rooftop play a significant role?

Section II describes the measurement concept and equipment. In Section III we present the validation of the used technique. Section IV introduces the measurement environment and Section V shows some sample results. In Section VI we discuss our classification of propagation mechanisms, and finally, Section VII summarizes and concludes this work.

II. Measurement Concept and Equipment

A. General

Measurements of the spatial radio channel require a multi-channel sounder that is able to receive signals from all array elements coherently. The channel description functions (e.g. impulse responses) can then be calculated by using

J. Laurila is now with Nokia Research Center, Radio Communications Laboratory, Helsinki, Finland. Together with M. Toeltsch, K. Hugl, and E. Bonek he was with Institut für Nachrichtentechnik und Hochfrequenztechnik (INTHF), Technische Universität Wien, Vienna, Austria. E. Bonek is also with the Forschungszentrum Telekommunikation Wien (FTW), Vienna, Austria. K. Kalliola and P. Vainikainen are with the Institute of Digital Communications (IDC)/Radio Laboratory, Helsinki University of Technology, Espoo, Finland. K. Kalliola is also with Nokia Research Center, Radio Communications Laboratory, Helsinki, Finland. E-mail: juha.k.laurila@nokia.com.

signal samples from different sensors which further allows the spatial characterization of the channel (e.g. resolving the directions of arrival, DOA). But, this multi-channel sounding approach is costly and complex.

A practical alternative is to connect the elements of the array via fast RF-switches to a single-channel sounder. Thus, sounding is performed sequentially for each sensor. This RF-multiplexing technique becomes feasible when the switching delays are very short, in the order of some nanoseconds. Spatial measurements using a single receiver with multiplexing have been reported e.g. in [10] and [11].

The synthetic aperture technique is widely used in spatial channel measurements. The idea is to collect data from different spatial positions using a single receiving antenna. Arbitrary array geometries can be created by predefining an array aperture grid and moving a single sensor between these grid points. Another possibility is to move the receiver antenna with a constant speed and collect sounding periods at fixed intervals. The synthetic aperture technique has been applied to urban macrocell measurements at the BS site [4] and at the MS site [7], [8]. The basic requirement for this technique is that the channel remains constant during data collection over the whole aperture.

In this work we used a sounding method, combining RF multiplexing of physical array elements and the synthetic aperture technique.

B. Construction of Synthetic Array

The physical array consisted of 16 dual-polarized patch antennas that were installed above each other on a trolley with vertical and horizontal orientation of polarization axes. They were arranged in a zig-zag pattern and their spacing was $\lambda/2$ in both directions. This structure reduced the mutual coupling between the elements because the smallest inter-element distance was between the corners of the patches. 3dB beamwidth of elements was 70° with both polarisations.

The trolley moved with a constant speed of $0.3\,m/s$ over metallic rails to collect "snapshots" over the physical array at certain horizontal positions. Each snapshot corresponded to one column in the grid of the synthetic planar structure. We took the subsequent snapshot when the trolley had moved to the next horizontal position of the grid (distance between snapshots was $\lambda/2$) and continued until $N = 58$ snapshots in different horizontal positions were taken. Thus, the physical dimensions of the synthetic aperture were 8×29 wavelengths.

Figure 1 shows the measurement equipment at the microcell site.

C. Wideband Channel Sounder

We used the wideband channel sounder developed at Helsinki University of Technology by the Institute of Radio Communications (HUT/IRC) [12] with a carrier frequency of $2154\,MHz$. The RF bandwidth of the system is $100\,MHz$. The sounder uses the direct sampling technique, i.e. the samples from the I and Q receiver branches are collected directly to the memory. The impulse responses are produced by correlating the PN sequence of the transmitter and received signal samples (collected with oversampling rate of 4) using post-processing. The chip frequency of the system is $30\,MHz$. Thus the used m-sequence with a length of 255 leads to the maximum delay of $8.5\,\mu s$ with a resolution of $33\,ns$. This delay range is adequate in an European urban environment where really high-rise buildings do not exist.

The used RF-multiplexer has a switching delay of $3\,ns$. Thus, the snapshot collection period over the physical array was purely defined by the chip frequency and the code length. The data collection from all of the 16 dual-polarized elements lasted $1\,ms$. The uncertainty introduced by the constant movement of the trolley is negligible (the trolley moves only $1.6 \cdot 10^{-4}\,m = \lambda/900$ during a snapshot collection period).

The transmitter and the receiver used rubidium standards with long-term phase stability of $2 \cdot 10^{-11}$ as a frequency reference. The synchronization was checked before and regularly during a measurement session using a line of sight (LOS) measurement. This guaranteed the phase stability of transmitter and receiver in all measurement positions.

D. Post-Processing of Data

After calculating the impulse responses of all synthetic sensor positions we reorganized the data so that the post-processing could be performed for a normal planar structure (elimination of the zig-zag shape). The angular response was resolved from the spatially separated impulse responses by using 2-D Unitary ESPRIT [13], a subspace based super-resolution method. The number of antenna elements does not directly influence the resolution, while it is crucial for the maximum number of distinguishable waves. A more thorough description of the data evaluation method can be found in [7] and [8]. In this paper we summarize only the basic principle.

¿From the impulse response averaged over all synthetic aperture elements, we selected all delay samples with power above a threshold value. Depending on the transmitter position, and therefore on the SNR, the dynamic range between the strongest impulse response peak and the selected threshold value varied between 15-30 dB. Mostly it was above $25\,dB$. Dynamic range was optimised by visual inspection separately for each transmitter position. For each selected time instant we estimated L DOAs by 2-D Unitary ESPRIT [13] after 2-D spatial smoothing [14]. Varying L, we were able to select the optimal number of DOAs, L_{opt}, by minimizing the so-called data estimation error, ϵ_D. This error is defined as the difference between the measured received signal and its reconstructed counterpart that is based on the DOA estimates. ¿From these DOA values we created the corresponding array steering matrix and performed

beamforming to estimate the power of impinging waves. The estimation procedure described above was carried out separately for received vertically and horizontally polarised components. Thus, as the output of post-processing we obtained for both polarisations the number of incoming waves for each active delay sample followed by the azimuth and elevation angles, and corresponding powers for each of them.

III. Validation of the Measurement Concept

The basic requirement for synthetic aperture measurements is that the channel does not change during the whole data collection period. Therefore, the measurements were performed during night with minimum traffic. The snapshots in the different horizontal positions of the array were taken with intervals of $0.2\,s$, which leads to a total data collection period of $14.5\,s$. Note that this period is short compared to the case when one single antenna is moved manually over the grid points of the synthetic aperture. Thus, our technique sets less requirements on the coherence time of the channel. Note also that any possibly moving objects, which might cause reflections, were not in the vicinity of the array.

We tested the effect of traffic (moving cars in the vicinity of the transmitter) by taking two independent measurements at the same TX position

1. without traffic (TX18/RX3),
2. with and without traffic (TX10/RX3),
3. with traffic (TX12/RX3).

Then we evaluated the power in the dominating cluster as explained in Sec. VI-A. Case 1 shows a maximal cluster power variation of 5% over the consecutive measurements compared to the total received power. Cases 2 and 3 show a variation of max. 20% of the total power. From these results we can conclude (i) that the repeatability of measurements is good in the absence of traffic, whereas (ii) moving objects (e.g. cars) do have an effect. All our evaluations in the sequel are based on measurements without traffic.

We also used LOS measurements with an exactly known transmitter position to validate the accuracy of the concept. By comparing the estimated azimuth and elevation angles to the geometrically calculated values we were able to ensure the proper operation of the system during the whole measurement session. The estimated LOS DOAs corresponded to the real values within an estimation error of less than 1°. This error is mainly caused by practical inaccuracies of the measurement configuration (like wind load on the physical array or rail misalignment). Additionally, considering the phase variation of the LOS component over the physical and synthetic aperture allowed to check the calibration of the array and the velocity of the trolley, respectively.

We eliminated the deviation of the pattern of the individual patch elements from omnidirectional after the DOA estimation step. We multiplied the estimated power of incoming paths by the inverse of the measured antenna pattern in the corresponding direction. The antenna pattern of the elements is nearly flat up to an azimuth angle of 40° and shows a fast drop beyond (gain reduction $\approx 4\,dB@40^\circ$). To guarantee the reliability of the pattern correction, we discarded any components arriving from outside of the azimuthal range of $\pm 60^\circ$.

IV. Measurement Environment

We carried out the measurements in an urban environment in downtown Helsinki. We used three receiver array sites (in different positions), RX1 below rooftop at the third floor level ($h_{RX} = 10\,m$), RX2 at rooftop level ($h_{RX} = 27\,m$) and RX3 above rooftop level ($h_{RX} = 21\,m$). The height of other buildings in RX3 measurement sector is rather low, and thus already h_{RX} of $21\,m$ is enough to raise receiver array above the other rooftops. These receiver positions correspond to real micro- and macrocell antenna installations in urban environments. Figure 2 shows the map of the area covered by all RX sites including the transmitter positions.

At the RX1 site the environment is relatively open. In front of the array is the railway station with an open and flat railway yard behind it. The open square (Rautatientori) dominates the environment to the right of the antenna broadside (see Fig. 3). There is a park behind the first block on the northern side of the square, which reduces the number of reflections from that direction. The main entrance of the railway station with large windows is on the street level about 40° left from the antenna broadside and a station tower is directly in front of the array (0°). Our transmitter was mostly in the narrow street canyons or on the railway yard behind the station building.

A characteristic environmental feature for the second receiver position (RX2) is the broad street (Kaisaniemenkatu) approaching the receiver from the left with an angle of about 30° from broadside (see Fig. 4). The open square in the vicinity allowed coupling of the energy to this street in most cases. The height of buildings beside and in front of the array is equal to the antenna height. Only two buildings on the northern side of the square rise slightly above the environment (Theatre Tower, White Tower, see Fig. 3) and there is a LOS between them and the receiver array. The transmitter was positioned on the square and in different types of street canyons leading to different physical propagation conditions.

The third receiver site (RX3) was on the roof of the Pukeva parking house clearly above the rooftops of the buildings in the measurement sector. At an angle of about 40° to the right of the broadside there is the Lutheran Cathedral towering clearly above the surroundings (Fig. 5). On the southern side of the cathedral there is an open square (Senate Square)

without a LOS connection to the base station. The transmitter positions were in different types of street canyons and on the square.

Figure 3 shows the view from the RX1 (microcell) site towards the open square, Fig. 4 from the RX2 site (macrocell) towards the street and Fig. 5 from the RX3 site (macrocell) towards the cathedral.

The RMS delay spread values, DS, obtained in our measurements are in agreement with values from literature for urban areas. For the three RX sites mean DS values, averaged over transmitter positions, were $1.27\,\mu s$, $1.19\,\mu s$ and $0.65\,\mu s$, and the values ranged between 0.69-2.32 μs (RX1), 0.53-2.37 μs (RX2) and 0.31-2.04 μs (RX3).

The distances between RX and TX sites varied between $100\,m$ and $500\,m$. Even if the antenna installation of RX2 and RX3 sites corresponds to macrocells, we were not able to measure propagation distances corresponding to radii of the biggest urban macrocells. This was due to limitations caused by the measurement system. However, our measurement distances are in line with many current urban site configurations. The corresponding angular range of the TX positions, seen by each RX site, was $-45 \ldots +45°$. The transmitter was always positioned on street level with the antenna height of $1.5\,m$ corresponding to a normal mobile station. For transmission we used a vertically polarized discone antenna with omnidirectional pattern in the azimuthal domain (3dB elevation beamwidth 87°).

V. Sample Results

During the measurement campaign we collected data from over 70 different transmitter positions. We first introduce some sample results. We selected cases where several distinct propagation mechanisms became evident and which are representative for the whole set. To make the interpretation of the results easier, we grouped the incoming waves according to their physical propagation routes. We call these groups *clusters* and identify them in the sample result figures. If clusters were close to each other in either one of the azimuth, elevation or delay domains, we separated them if they had different propagation routes. The names of the clusters are given in *italic* in the text and the corresponding propagation routes are pointed out in the maps and photos. Our sample plots show the sum power of the received vertically and horizontally polarized components over azimuth, elevation, or delay planes. We selected the delay window so that the first incoming waves arrive with small excess delays. Thus, all delay values shown are relative, not absolute. The darker colors of the contour plots indicate higher received power.

A. RX1 - Array below Rooftop (Microcell)

A.1 Transmitter Position TX11 (RX1)

The transmitter position TX11 (RX1) was located in the street behind the block on the northern side of the 'Rautatientori' square. Figure 6 shows a detailed map of the surroundings of the transmitter and Fig. 7 and Fig. 8 azimuth-elevation and azimuth-delay planes, respectively. The narrow street canyons on both sides of the theatre building (Fig. 3, Fig. 6) dominate this propagation scenario. Most waves arrive with low elevation angles from these azimuthal directions (*street1 - street2*). The environment also shows spreading in the delay domain, which corresponds to reflections from the park (north of the transmitter) and multiple reflections in the street canyons. The objects on the square cause some reflections and the receiver sees these components, with low elevation angles, in the azimuthal range between 10° and 50°. We observe also weak diffracted components with high elevation angles from the *theatre tower*.

A.2 Transmitter Position TX6 (RX1)

The transmitter position TX6 (RX1) was situated in the railway yard near the entrance of the station building. Figure 9 shows a detailed map of the environment of TX6. Figures 10 and 11 show the received power over elevation-delay and azimuth-elevation planes, respectively. The main entrance of the station with large windows is on the opposite side of the building. These two entrances are connected by a wide corridor. The first components in the delay domain propagate through the building and they are seen at the receiver with a low elevation angle and azimuthal angle of about $-40°$ (*station entrance*). These components show short spreading in the delay domain. The propagation over the roof begins almost simultaneously (*over rooftop*). The first components of this cluster originate over the roof of the direct path diffraction. Also more delayed waves reflected from the objects in the railway yard exist. In addition to the diffraction over the roof we also see a reflected component from the metallic cupola of the station tower (Fig. 3, Fig. 9). This component (*tower*) has a high elevation of 21° and it carries a lot of power. Several reflectors exist in the street canyon below the receiver array and thus we observe delayed components with low elevation angles in the azimuthal range between 0° and $-20°$. These are related to multiple reflections from the street and the wall of the station building (*street canyon*). It might also be possible that some of these waves experience multiple reflections inside the station and impinge on the receiver through the windows of the building.

A.3 Typical Behavior of RX1 Site

Figure 12 shows the azimuth power spectrum (APS) averaged over all transmitter positions. The same clusters (*street1, street 2, station entrance, over rooftop,* and *street canyon*) already pointed out in sample results, are also

evident in this averaged chart. Figure 12 links our contour plots to the more conventional APS representations. As a typical result, we note that the APS has distinct peaks, irrespective of actual TX position. These peaks can be clearly attributed to objects in the propagation path.

B. RX2 - Array at Rooftop (Macrocell)

B.1 Transmitter Position TX5 (RX2)

The transmitter position TX5 (RX2) was situated near the north-eastern corner of the open square. Figures 13 and 14 show azimuth-elevation and elevation-delay planes, respectively. The first signal component arrives from the transmitter direction diffracted over the rooftop (*pseudo-LOS*). Only slightly delayed waves arrive from the azimuth angles around $25°$ and $30°$, which correspond to the reflections from the relatively high buildings on the northern side of the square (*theatre tower* and *white tower*) (see Fig. 2 and Fig. 3). The last over-the-roof components are propagated over the block in front of the array after some reflections on the square and on the roof (*chimney stack*). Simultaneously with these reflections, the first components from the direction of the 'Kaisaniemenkatu' (*street canyon*) begin to arrive. From this direction we see considerable dispersion in the delay domain because a lot of reflected components arrive from this azimuthal range. Note that these street canyon guided waves exhibit a strong correlation between elevation and delay. The signal components arriving with the shortest delays are diffractions from the corners of the street canyon, they show the lowest elevation. The elevation angle increases as a function of delay, because the later components are reflections from the objects further away (see Fig. 4). Some of the street canyon propagated components evidently experience local scattering near the base station, thus they have very low elevation angles of $-16°$ (*street canyon scattering*).

B.2 Transmitter Position TX28 (RX2)

The TX28 (RX2) position exhibits an interesting special effect. The transmitter was positioned in the street canyon of 'Aleksanterinkatu' about 500m southeast from RX2. There is a LOS connection between the transmitter and the highest building in the surroundings, which rises clearly above the other ones. The top of this building has also a LOS connection to the RX site (see Fig. 4).

Figures 15 and 16 show the power delay profile and delay-azimuth plane, respectively. The waves reflected from the building (*Hotel Torni*) arrive about $1.5\,\mu s$ after the first components and show the strongest power. For the waves with shorter delays, two different propagation mechanisms exist. One component propagates over the rooftop with the azimuth angle of $-45°$. The relatively high-rising 'World Trade Center, (WTC)' building seems to block all components in the azimuthal range between $-35°$ and $-45°$. The energy of the cluster (*WTC corner)* originates from a diffraction at the left corner of the WTC building. Another significant short delay component is related to the coupling of the signal energy to the street canyon of 'Keskuskatu'. The signal is observed at the receiver after reflections from the 'Makkaratalo' building (see Fig. 4).

B.3 Typical Behavior for RX2 Site

Figure 17 shows the sum power in the azimuth-elevation plane averaged over all transmitter positions. Remembering that RX2 position is at rooftop level, it shows a surprising result: independent of the transmitter position the same propagation mechanism dominates, i.e. we always observed strong signal components from the direction of the street-canyon. Often reflections from the towers on the northern side of the square appeared as well. Only the relative delays between these dominating clusters varied with different transmitter positions. The dominating clusters (*street, white tower, theatre tower*) are clearly visible in the averaged response of Fig. 17. Over the roof propagation is weak. We conjecture that the open square reinforces this "tunneling" effect because it allows coupling of energy to the street canyon of 'Kaisaniemenkatu' in most transmitter positions. We do not expect this behaviour so pronounced in a pure 'Manhattan grid' environment.

C. RX3 - Array above Rooftop (Macrocell)

C.1 Transmitter position TX3 (RX3)

The transmitter position TX3 (RX3) was situated in the relatively wide street of 'Snellmanninkatu' in the direction of $5°$ to the right from array broadside. The buildings on both sides of this street are relatively high. The two streets parallel to the array broadside (*street1* and *street2*) dominate this propagation environment. Some energy arrives by diffraction over the rooftop, but the components propagating along the street canyon carry considerably stronger power. Note that also the components propagated over the roof show negative elevation angles due to the receiver position being clearly above the other buildings. The elevation of the 'Snellmannninkatu' street level is -5°. The components propagated in the cluster *street2* arrive slightly later and show shorter spreading in the delay domain than their counterparts in the cluster *street1*. The interesting special effect related to the *street2* propagation is the diffraction from the edge of the 'Bank of Finland, (BOF)' building. With the transmitter positions TX2-TX8 we often observed relatively strong

components from the azimuth angle of 25° and in the elevation range between $-7°$ and $-2°$, which originate from this diffraction.

The Lutheran Cathedral, especially its metallic cupola, acts as a reflector carrying significant components with high elevation angles. This cluster (*cathedral*) shows also some spread in delay, which means that the components have gone through different propagation routes before the final reflection from the cathedral. We do not show any plots for TX3 because all the effects discussed here are also present in the averaged response of Fig. 19.

C.2 Typical Behavior for RX3 Site

Figure 18 shows a detailed map of the RX3 environment. Figure 19 demonstrates the typical effects observed at RX3 site by showing the sum power in the azimuth-elevation plane averaged over the transmitter positions TX2-TX8. The clusters (*street1*), (*street2*), and (*cathedral*) are clearly visible.

The cathedral is a dominating object in this environment and some reflections from it are observed almost always, independently of the transmitter position. Dominant reflectors act as pseudo signal sources carrying waves with different delays to the receiver. This effect was especially pronounced when the transmitter was on the square (on the southern side of the cathedral). The geometrically shortest path between TX and RX does not necessarily occur at all.

VI. Classification of Propagation Mechanisms

Our sample results (Ch. V) showed some dominant, well identifiable *clusters* in the azimuth-elevation-delay domain that were present at all transmitter positions. The high resolution of our measurement and post-processing techniques allows the identification of the position of the final reflection or diffraction. The delay, in combination with street maps, gives clues to whether the waves undergone simple or multiple bounces on their travel from transmitter to receiver. Based on this information we were able to allocate each cluster to a certain *propagation class*. Also, quantitative assessment of the relative importance of different propagation mechanisms becomes possible. In the analysis, we used the following three *propagation classes*:

- *Street-guided propagation (Class 1)*: The waves arrive the receiver from the street-level. Typically clusters arriving from the square (RX1) or from the direction of the street canyons (RX2, RX3) belong to this class.
- *Direct propagation - over the rooftop (Class 2)*: The clusters of this class have high elevation angles. The energy is typically arriving from the direction of the transmitter with some spreading in azimuth and delay domains. These clusters are present e.g. in transmitter positions TX3-TX7 (RX1) and TX10-TX20 (RX3).
- *Scattering from high-rise objects - over the rooftop (Class 3)*: All clusters that are received over the rooftop after reflection from clearly identifiable high-rise objects belong to this class. Typically e.g. the towers of the railway station (RX1), theatre (RX2) and cathedral (RX3) act as such objects.

In case that the history of some waves is a mixture of different propagation classes (e.g. over the rooftop diffraction preceding propagation in the street canyon), we allocate such clusters to their last class (to the class *street guided* in our example). Note that unambiguous identification of the complete history of waves would require double-directional measurements [15].

A. Definition of cluster powers

We calculated the power carried in each cluster and averaged these cluster powers for each propagation class by using the following procedure. For each transmitter position we determined azimuth elevation delay power spectrum (AEDPS) and plotted three sections in the azimuth-elevation, azimuth-delay and elevation-delay planes. We showed some results of this analysis in Ch. V (Sample Results). By visual inspection we defined cluster borders in all three domains (azimuth, elevation and delay). Having these cluster definitions available, we summed up the power of all waves within these borders. In the delay domain we selected only such impulse response taps that carried significant power above the selected threshold. They are the same taps as used in the DOA estimation with 2-D Unitary ESPRIT (Ch. II-D). We obtained the cluster powers for vertical and horizontal polarizations separately.

The accuracy of our clustering procedure was verified by comparing the sum of the cluster powers and the total received power over the whole considered angular range for each transmitter position. These values fit very well; for 80% of the transmitter positions the difference was less than $1.5\,dB$. This guaranteed that the power impinging from outside our identified clusters is negligible. Furthermore this demonstrates that the received power is strongly concentrated in the identified clusters.

B. Relative Class Powers

To quantitatively assess the relative importance of propagation mechanisms, we summed up the powers of the *clusters* belonging to each *propagation class* and compared these values to the total received power. Table I shows these relative class powers for each receiver site separately for vertical and horizontal polarizations. Values are averaged over all transmitter positions of each RX site. At RX1 and RX2 sites, Class 1 (*street-guided propagation*) dominates with over 90% of the total power. Especially the 'Kaisaniemenkatu' street aperture delivers more than 95% of the power (RX2).

RX	Class	P_{class}/P_{tot} [H pol.]	P_{class}/P_{tot} [V pol.]
1	1	96.5%	95.7%
	2	2.4%	3.8%
	3	1.1%	0.4%
2	1	93.5%	97.2%
	2	4.0%	2.7%
	3	2.5%	0.1%
3	1	46.7%	78.0%
	2	37.2%	12.8%
	3	16.0%	9.2%

TABLE I
AVERAGED CLASS POWERS OF RX1, RX2, AND RX3

Propagation over the rooftop (Class 2 and 3) does not play a significant role for RX1 and RX2. At the RX3 site (which is above the rooftop level) the power of Class 1 reduces to 75%, while Class 2 and Class 3 powers rise accordingly. Class 3 power consists almost completely of reflections from the Lutheran Cathedral. Without the cathedral, the power of these clusters would have decreased to almost zero.

C. Polarization

Comparing the received cluster powers in both polarizations we directly obtain the cross-polarization discrimination (XPD) for the vertically polarized transmitted signal. XPD values were calculated for each cluster carrying received power levels clearly above noise floor with both polarizations. Figure 20 shows the cumulative distribution function (CDF) of the clusters' XPD values. The mean XPD value over all clusters was $8.0\,dB$. The shape of the CDF demonstrates that the co-polarized vertically received component dominates in the urban environment. A similar result was reported in [16] where different antenna configurations were compared.

An interesting depolarization effect was observed from strong specular reflections off round metallic objects (cupolas of the cathedral (RX3) and the station tower (RX1)). Such reflected components showed low or even negative XPD values – the mean XPD for such reflections was $-1.7\,dB$. In other words, the received cross-polarized components were significantly stronger than in the case of multiple reflections or diffraction. RX3-CDF of Fig. 20, where the probability of values less than $0\,dB$ is significantly higher than for other RX sites, demonstrates this effect. The more detailed investigations of this interesting behavior are outside of the scope of the current paper and we will leave them as a topic for further work.

VII. SUMMARY AND CONCLUSIONS

Our results show that the energy arrives to the base station from identifiable *clusters* in the azimuth, elevation and delay domains. These clusters correspond to different physical propagation routes and mechanisms, such as street-guided propagation with multiple reflections from the street canyon walls or single reflections from dominant objects. Grouping of these clusters to *propagation classes* allows a quantitative analysis of the propagation mechanisms for different receiver array installations. Our classification into three classes (*street-guided propagation (Class 1), direct propagation - over the rooftop (Class 2)* and *Scattering from high-rise objects - over the rooftop (Class 3)*) is comprehensive – we were able to allocate each of our clusters to one of these three classes.

The propagation scenario is determined by the environment seen by the base station. Street canyons that are essentially parallel to array broadside guide the waves to the BS. The main part of the energy was always received from the direction of a street aperture, independently of the position of the transmitter. This is true even if the receiver array is above rooftop level.

For the studied measurement distances ($100-500\,m$), the street-guided propagation clearly dominates over propagation over the building roofs. When the receiver was below or at the rooftop level (RX1, RX2), up to 97% of the total received power belonged to propagation class *street-guided propagation*. But also when the receiver was above the rooftop (RX3), the street canyons carried the strongest power (*street-guided propagation* $\approx 70\%$ of energy). Directly diffracted components, arriving with the shortest delays from the transmitter direction, were mostly weak and for many transmitter positions they did not appear at all.

Buildings rising above the average rooftop level typically act as reflectors or scatterers. Note that this was the case also in our relatively flat environment where real skyscrapers do not exist. Their effect is strongest if they have a LOS both to the transmitter and the receiver. Often such a dominant reflector acts like a pseudo signal source carrying waves with different delays to the receiver. Such components may have a different propagation history before the final

reflection from a dominant object. Their power is typically small compared to the total received power. Our results show that at most 9% of the power is carried by this propagation class.

We demonstrated the strong dependence between the environment seen by the base station and the propagation mechanisms in the typical urban environment. An accurate prediction of signal strength and quality at a specific base station site evidently requires advanced ray-tracing based simulation tools incorporating a building database with height information. The prediction of the signal and propagation routes will become even more important in the future, when network planning will be carried out for adaptive antenna base stations. The data set collected by our 3-D measurements would allow efficient evaluation and testing of such ray tracing tools.

What are the consequences for adaptive antennas? We comment on separate issues. First, we demonstrated that the received power is strongly concentrated in narrow azimuth and elevation ranges (clusters) in this urban environment, in contrast to the notion of widely spread angles of incidence. This finding is a prerequisite for adaptive antenna systems based on DOA estimation. On the other hand, the site selection for adaptive antenna base stations requires careful considerations so that interference suppression becomes possible. Positioning an adaptive array in front of a street aperture would be a poor choice in this sense. Radio resource allocation algorithms have to ensure that co-channel users are angularly well separated. But, note that the distance between transmitter and receiver was at most $500\,m$ in our measurements. With larger distances the impinging energy might be more concentrated to the direction of the transmitter due to propagation over roofs. This might improve interference suppression capability of adaptive antennas, especially with TDMA systems.

The results of our measurement campaign will also assist the parametrization of directional channel models. We have already contributed to the work carried out in the framework of the European COST 259 Action [17].

Acknowledgement: The authors would like to thank Martti Toikka, Lasse Vuokko and Viktor Nässi for their help during the measurement campaigns and colleagues of the INTHF/mobile communication group and IRC/radio laboratory for fruitful technical discussions. Special thanks to Dr. Andreas F. Molisch for several discussion and to Dr. Alexander Kuchar providing his direction of arrival estimation program. The measurements were carried out during two COST 259 short-term missions. This work was partially made in the framework of the projects funded by Austrian Science Fund (P-12147-ÖMA) and the National Technology Agency of Finland (TEKES/RAVE). Financial support of the Academy of Finland, Wihuri Foundation and Emil Aaltonen Foundation is also gratefully acknowledged.

References

[1] A. Paulraj and C. Papadias, "Space-time processing for wireless communications," *IEEE Signal Processing Magazine, no. 6*, vol. 14, pp. 49–83, Nov. 1997.

[2] R. B. Ertel, P. Cardieri, K. W. Sowerby, T. S. Rappaport, and J. H. Reed, "Overview of spatial channel models for antenna array communications systems," *IEEE Personal Comm.*, vol. 5, no. 1, pp. 10–22, Feb. 1998.

[3] U. Martin, J. Fuhl, I. Gaspard, M. Haardt, A. Kuchar, C. Math, A. F. Molisch, and R. Thomä, "Model scenarios for direction-selective adaptive antennas in cellular mobile communication systems - scanning the literature," *Wireless Personal Communications Magazine, Special Issue on Space Division Multiple Access*, vol. 11, no. 1, pp. 109–129, Oct. 1999.

[4] U. Martin, "Spatio-temporal radio channel characteristics in urban macrocells," *IEE Proc. Radar, Sonar and Navigation*, vol. 145, no. 1, pp. 42–49, Feb. 1998.

[5] K. Pedersen, P. E. Mogensen, and B. Fleury, "Dual-polarized model of outdoor propagation environments for adaptive antennas," in *Proc. of IEEE Vehicular Technology Conference (VTC'99), Houston*, pp. 990–995, May 1999.

[6] K. Pedersen, P. Mogensen, and B. Fleury, "A stochastic model of the temporal and azimuthal dispersion seen at the base station in outdoor propagation environments," *IEEE Trans. on Vehicular Technology*, vol. 49, no.2, pp. 437–447, Mar. 2000.

[7] J. Fuhl, J.-P. Rossi, and E. Bonek, "High resolution 3-D direction-of-arrival determination for urban mobile radio," *IEEE Trans. on Antennas and Propagation*, vol. 45, no. 4, pp. 672–682, 1997.

[8] A. Kuchar, J.-P. Rossi, and E. Bonek, "Directional macro-cell channel characterization from urban measurements," *IEEE Trans. on Antennas and Propagation*, vol. 48, no.2, pp. 137–146, Feb. 2000.

[9] K. Kalliola, H. Laitinen, L. Vaskelainen, and P. Vainikainen, "Real-time 3D spatial-temporal dual-polarized measurement of wideband radio channel at mobile station," *IEEE Trans. on Instrumentation and Measurement*, vol. 49, no.2, pp. 439–448, Apr. 2000.

[10] K. Kalliola and P. Vainikainen, "Characterization system for radio channel of adaptive array antennas," in *Proc. of Int. Symp. on Personal Indoor Mobile Radio Conference (PIMRC '97), Helsinki, Finland*, pp. 95–99, 1997.

[11] U. Trautwein, K. Blau, D. Brückner, F. Herrmann, A. Richter, G. Sommerkorn, and R. Thomä, "Radio channel measurement for realistic simulation of adaptive antenna arrays," in *2nd European Personal Mobile Communications Conference (EPMCC '97), Bonn, Germany*, pp. 491–498, 1997.

[12] J. Kivinen, T. Korhonen, P. Aikio, R. Gruber, P. Vainikainen, and S.-G. Häggman, "Wideband radio channel measurement system at 2 GHz," *IEEE Trans. on Instrumentation and Measurement*, vol. 48, no.1, pp. 39–44, Feb. 1999.

[13] M. Zoltowski, M. Haardt, and C. Mathews, "Closed-form 2-D angle estimation with rectangular arrays in element space or beamspace via unitary ESPRIT," *IEEE Trans. on Signal Processing*, vol. 44, no. 2, pp. 316–328, Dec. 1994.

[14] T.-J. Shan, M. Wax, and T. Kailath, "On spatial smoothing for direction-of-arrival estimation of coherent signals.," *IEEE Trans. on Signal Processing , no. 4*, vol. 33, pp. 806–811, Aug. 1985.

[15] M. Steinbauer, D. Hampicke, G. Sommerkorn, A. Schneider, A. F. Molisch, R. Thomä, and E. Bonek, "Array-measurement of the double-directional mobile radio channel," in *IEEE Vehicular Technology Conference (VTC2000-Spring), May 15-18, 2000, Tokyo, pp.1656-1662.*

[16] P. C. Eggers, J. Toftgård, and A. M. Oprea, "Antenna systems for base station diversity in urban small and micro cells," *IEEE Journal on Selected Areas in Communications*, vol. 11, no. 7, pp. 1046–1057, Sept. 1993.

[17] *COST Action 259 – Wireless Flexible Personalized Communications – Final Report.* European Commission, 2000.

Fig. 1. Measurement equipment

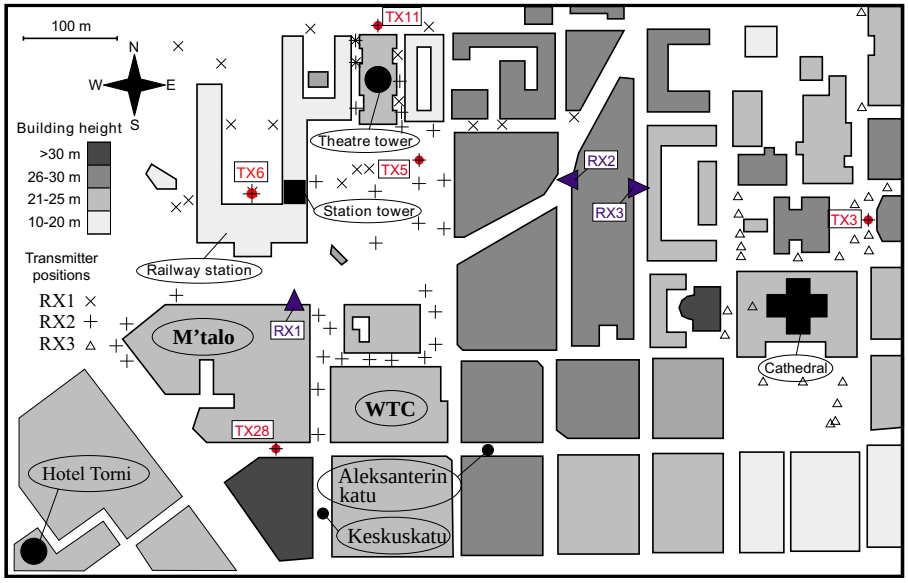

Fig. 2. Overview about the measurement area with all RX sites

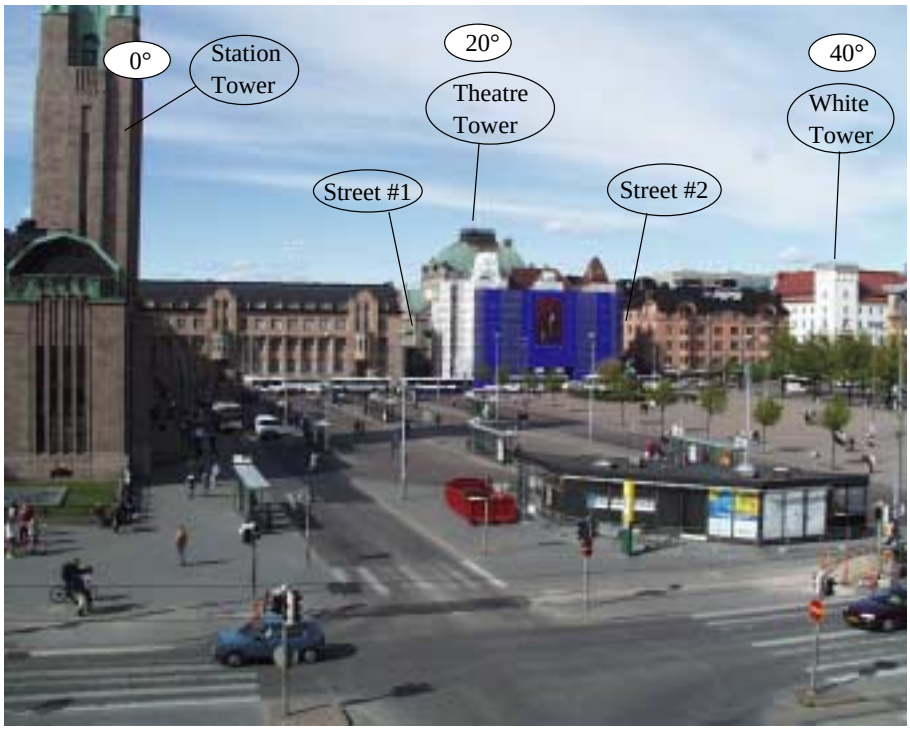

Fig. 3. View from RX1 site (microcell)

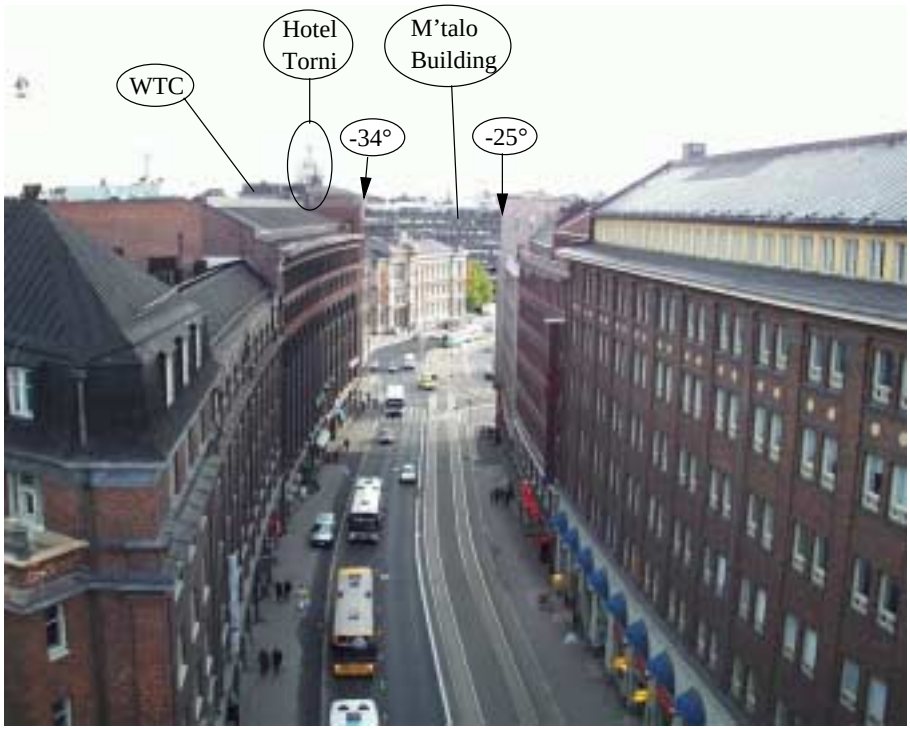

Fig. 4. View from RX2 site (macrocell)

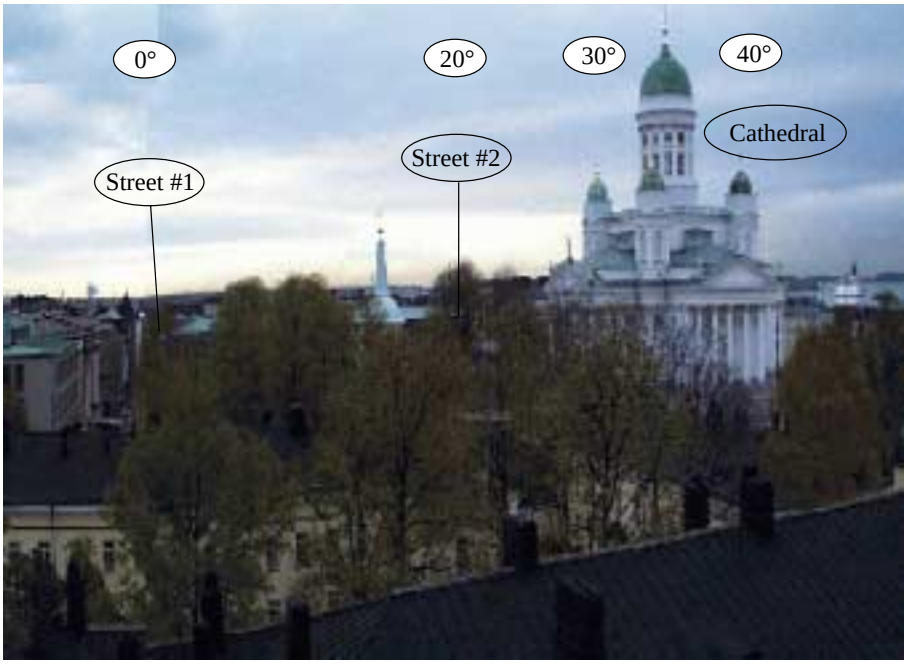

Fig. 5. View from RX3 site (macrocell)

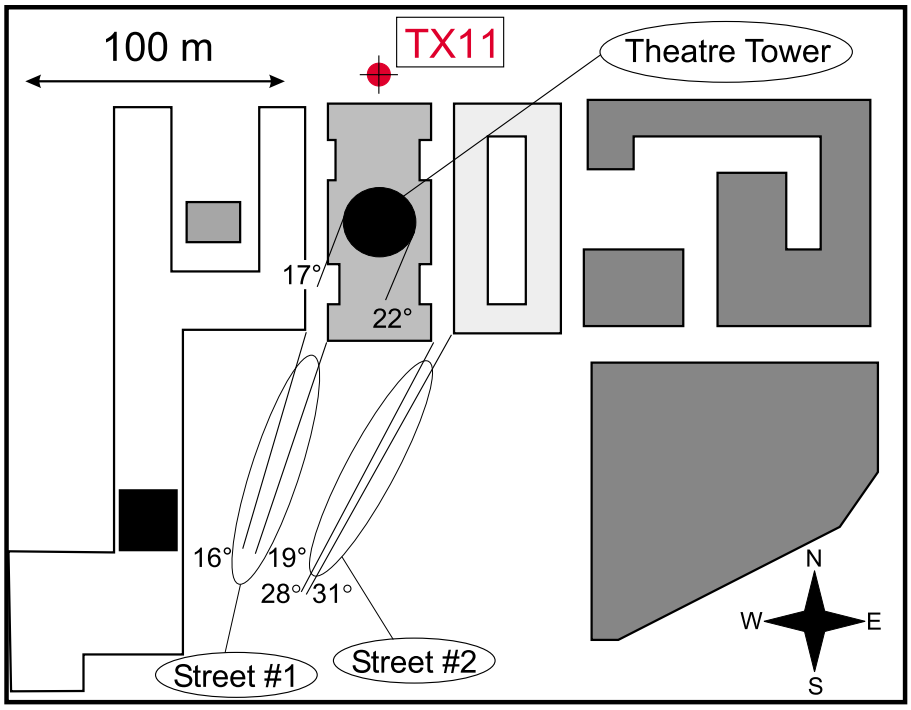

Fig. 6. TX11 (RX1): Detailed map

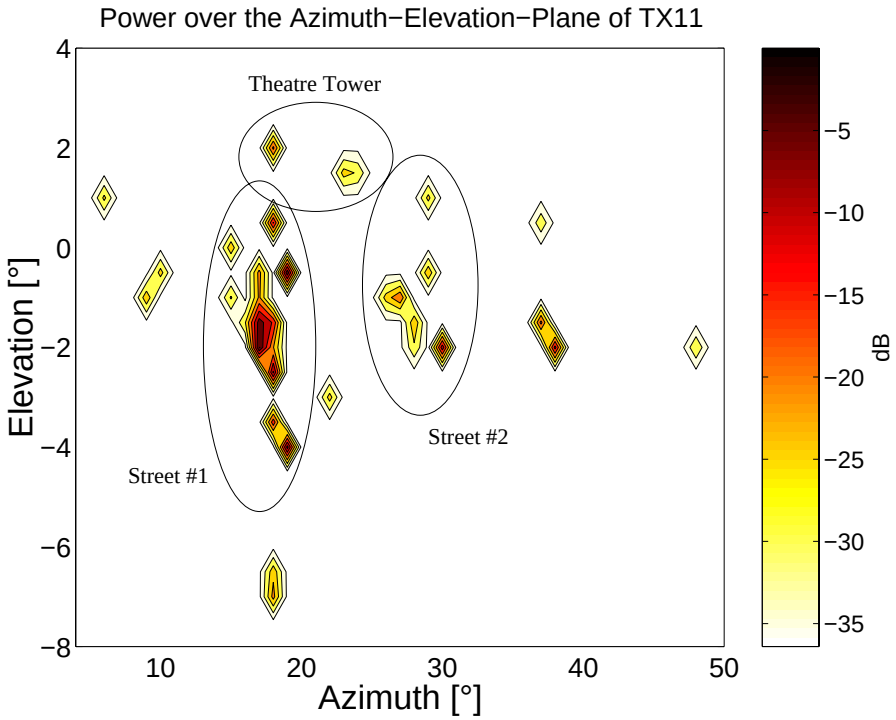

Fig. 7. TX11 (RX1): Azimuth-elevation plane

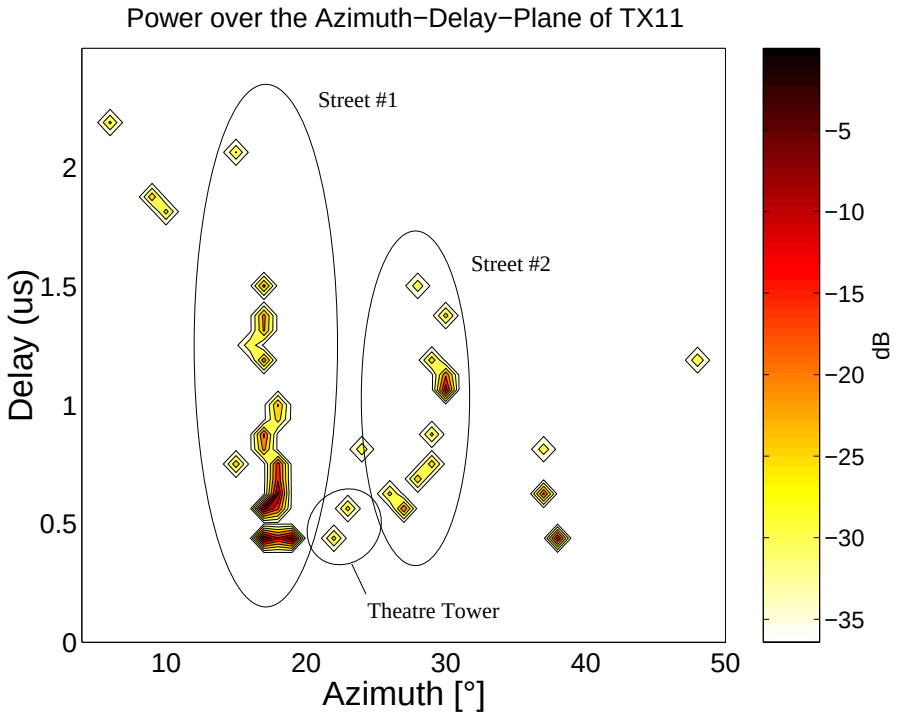

Fig. 8. TX11 (RX1): Azimuth-delay plane

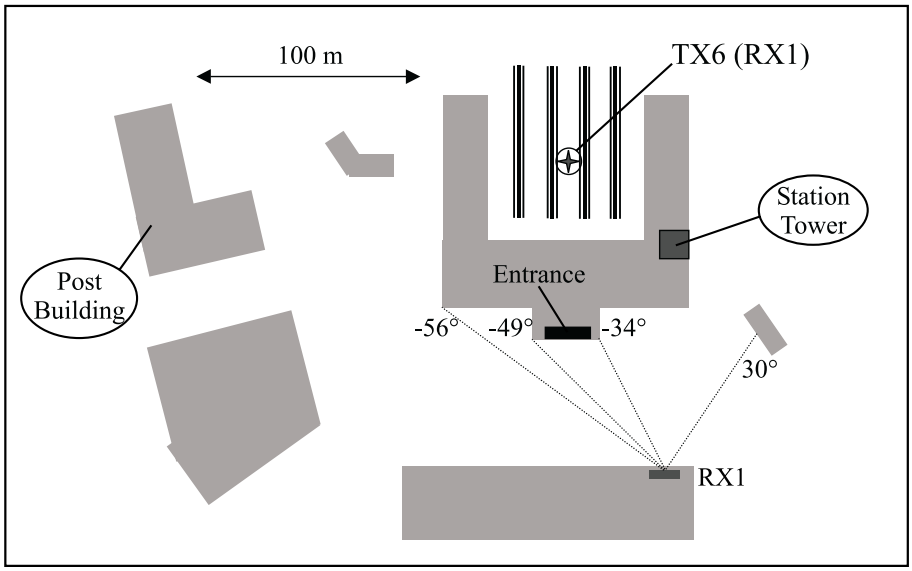

Fig. 9. TX6 (RX1): Detailed map

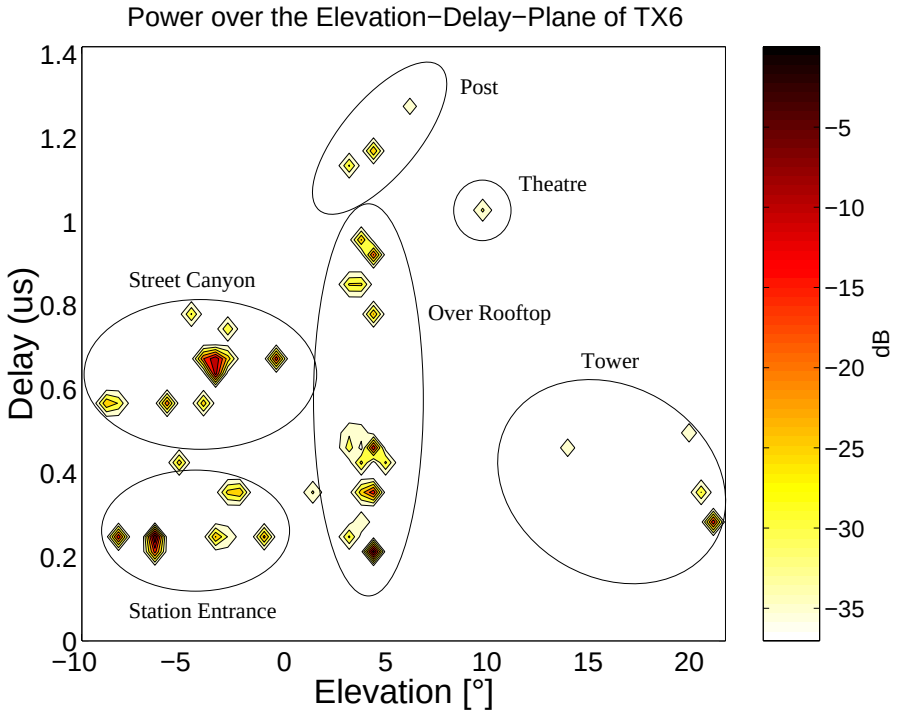

Fig. 10. TX6 (RX1): Elevation-delay plane

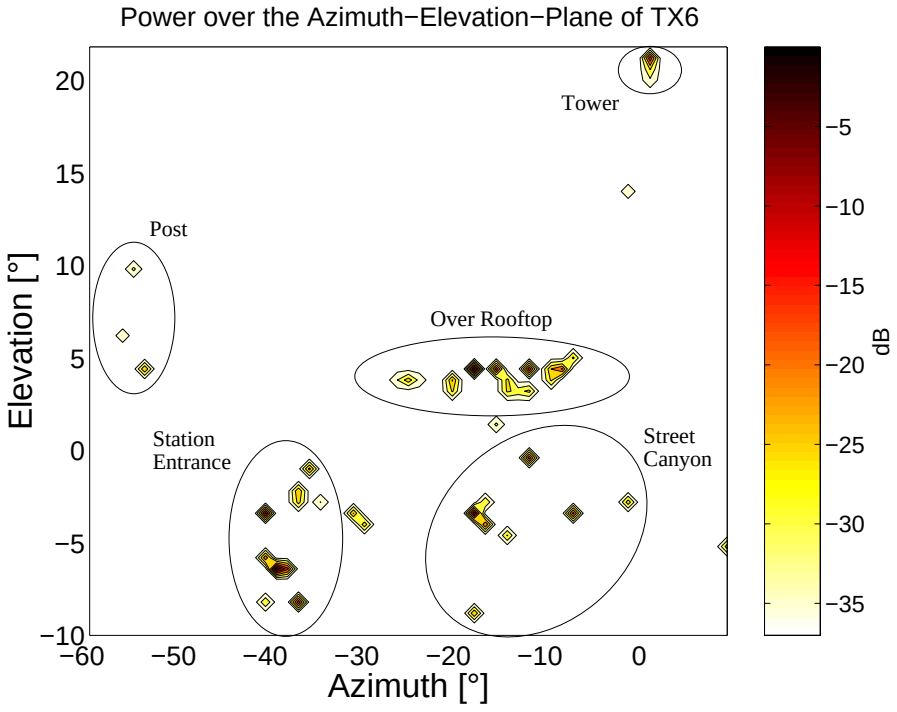

Fig. 11. TX6 (RX1): Azimuth-elevation plane

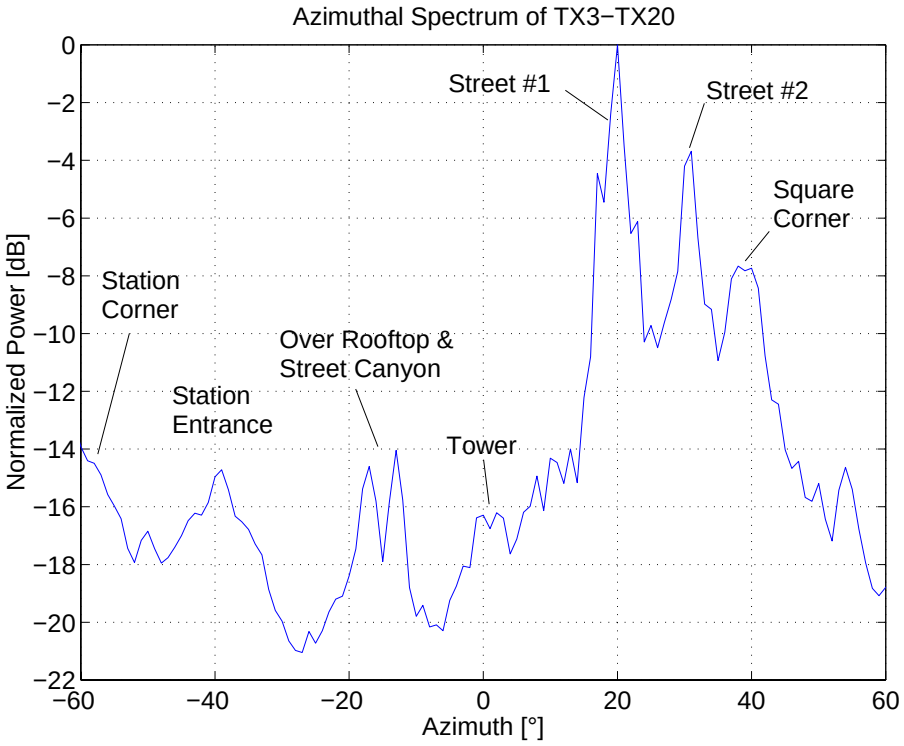

Fig. 12. TX3-20 (RX1): Azimuthal Power Spectrum

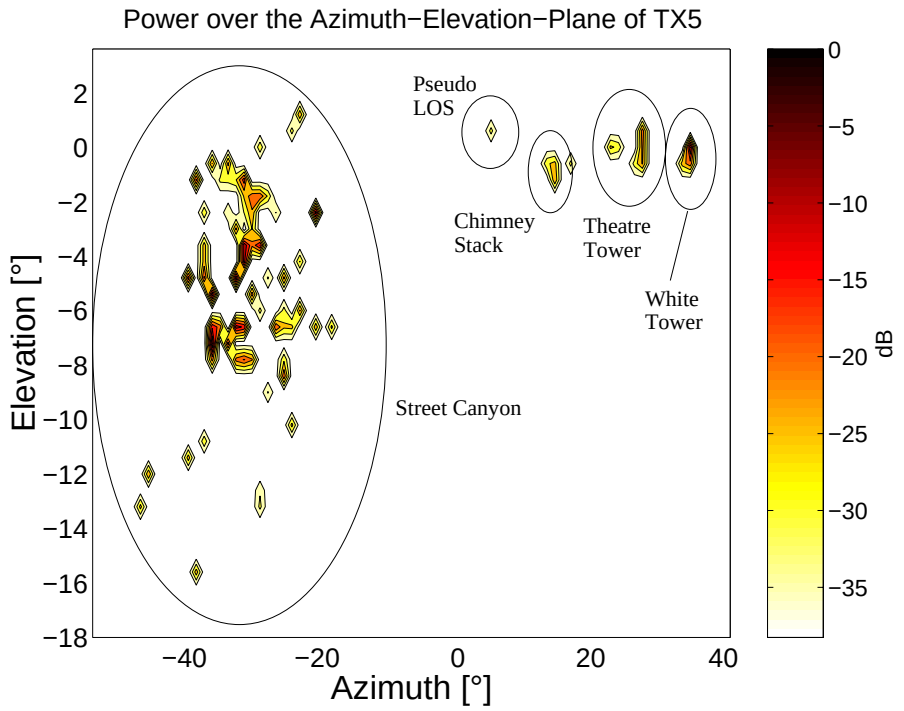

Fig. 13. TX5 (RX2): Azimuth-elevation plane

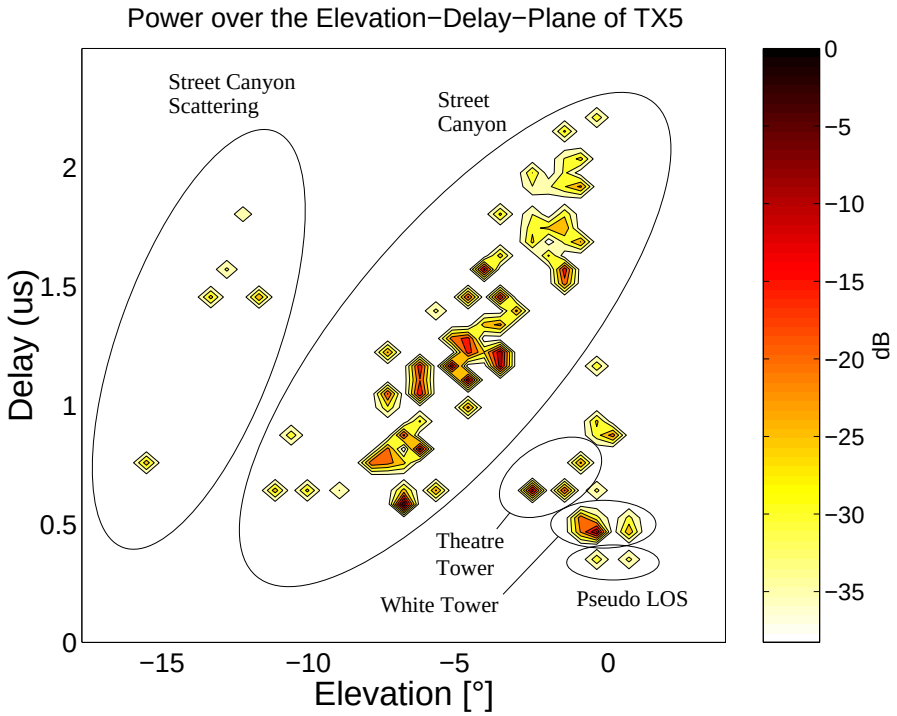

Fig. 14. TX5 (RX2): Elevation-delay plane

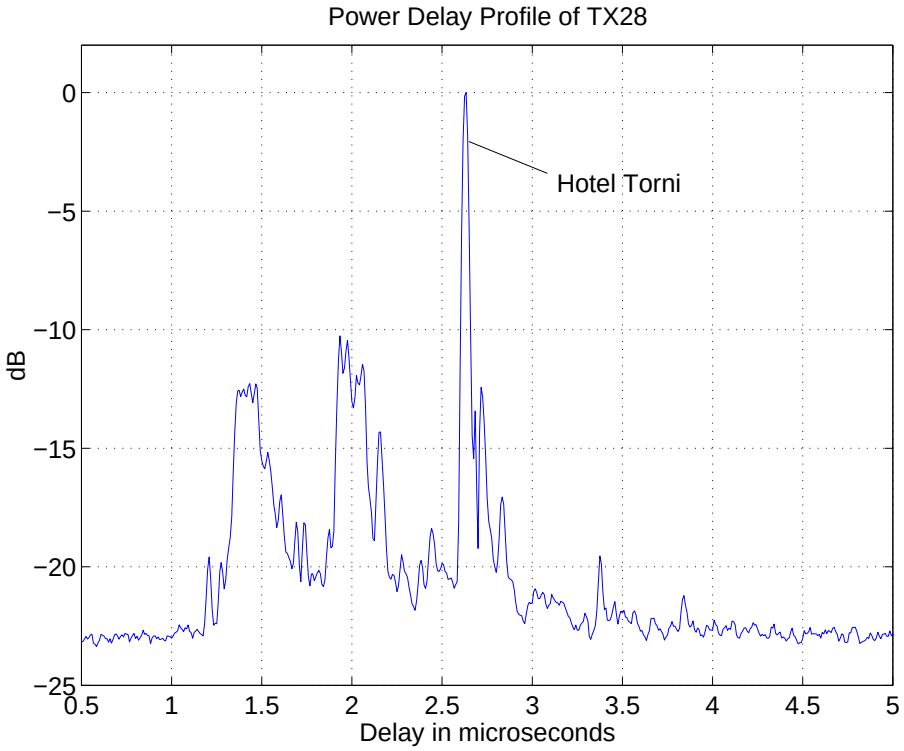

Fig. 15. TX28 (RX2): Power delay profile

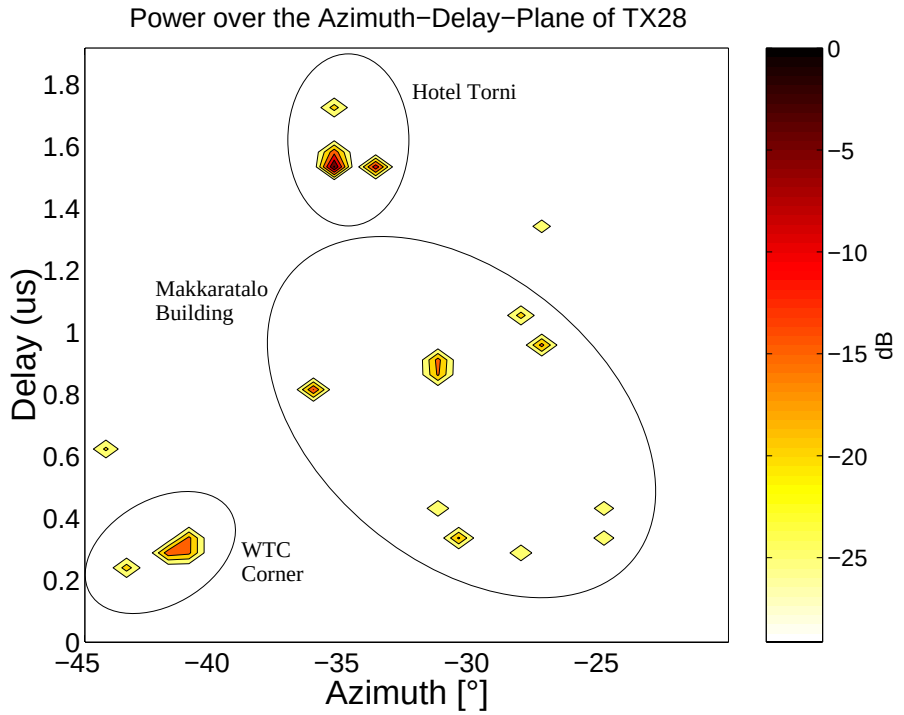

Fig. 16. TX28 (RX2): Azimuth-delay plane

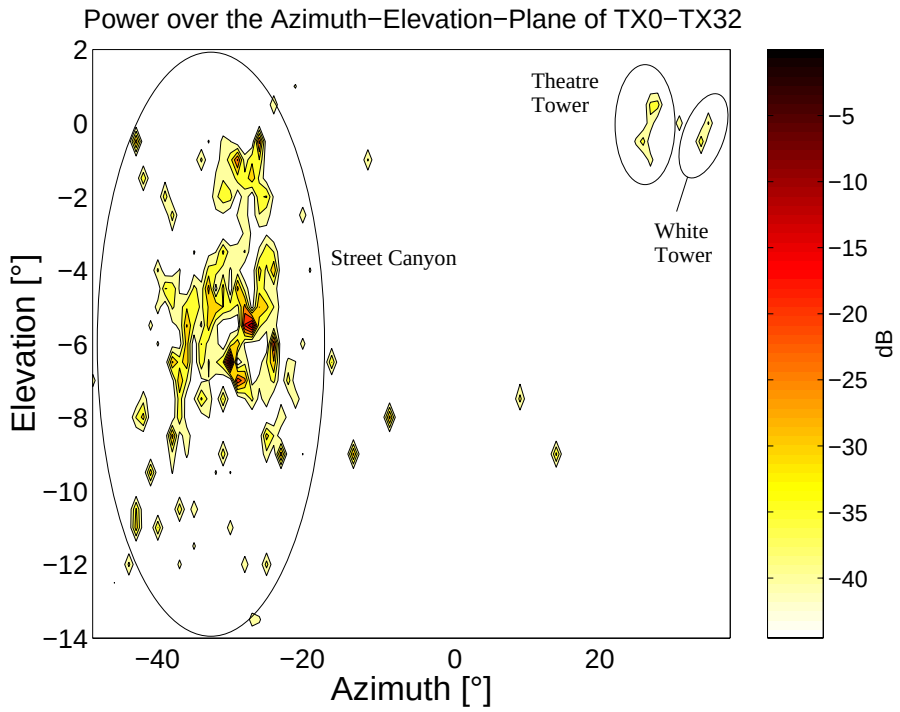

Fig. 17. TX0-32 (RX2): Azimuth-elevation plane

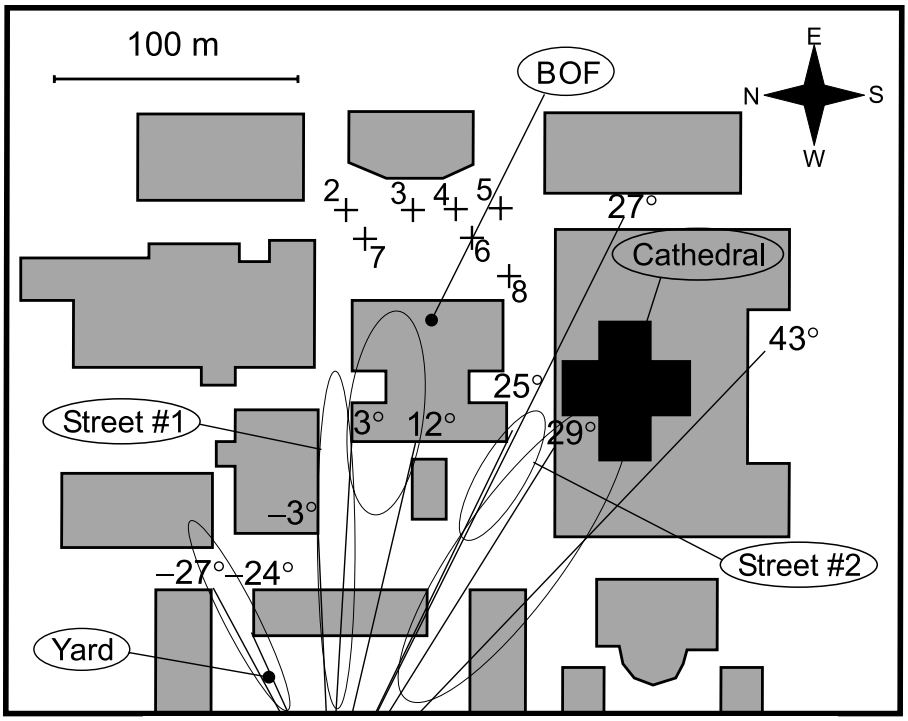

Fig. 18. TX2-8 (RX3): Detailed map

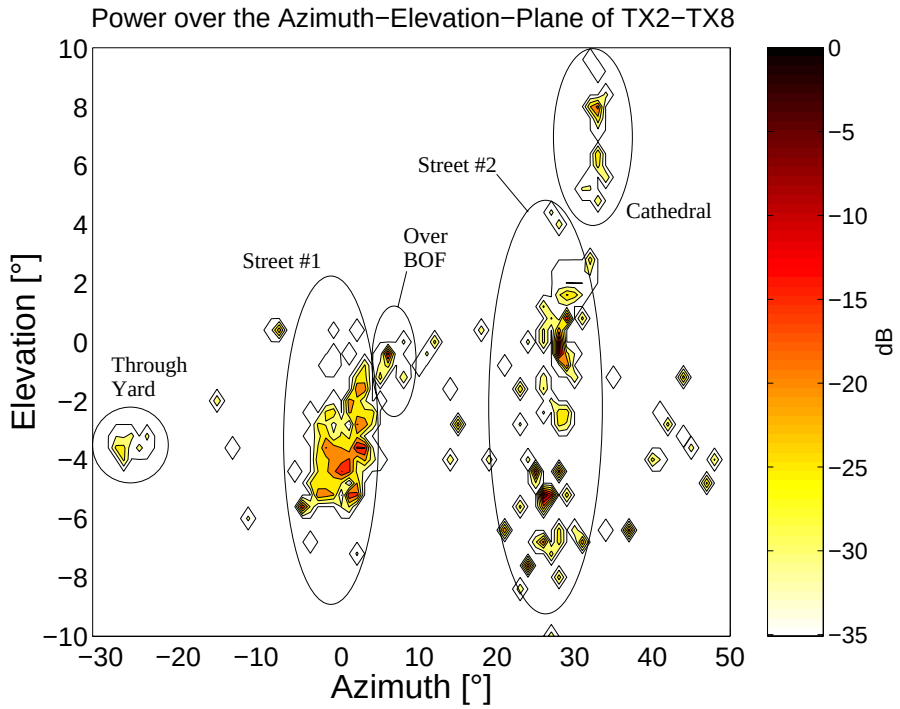

Fig. 19. TX2-8 (RX3): Azimuth-elevation plane

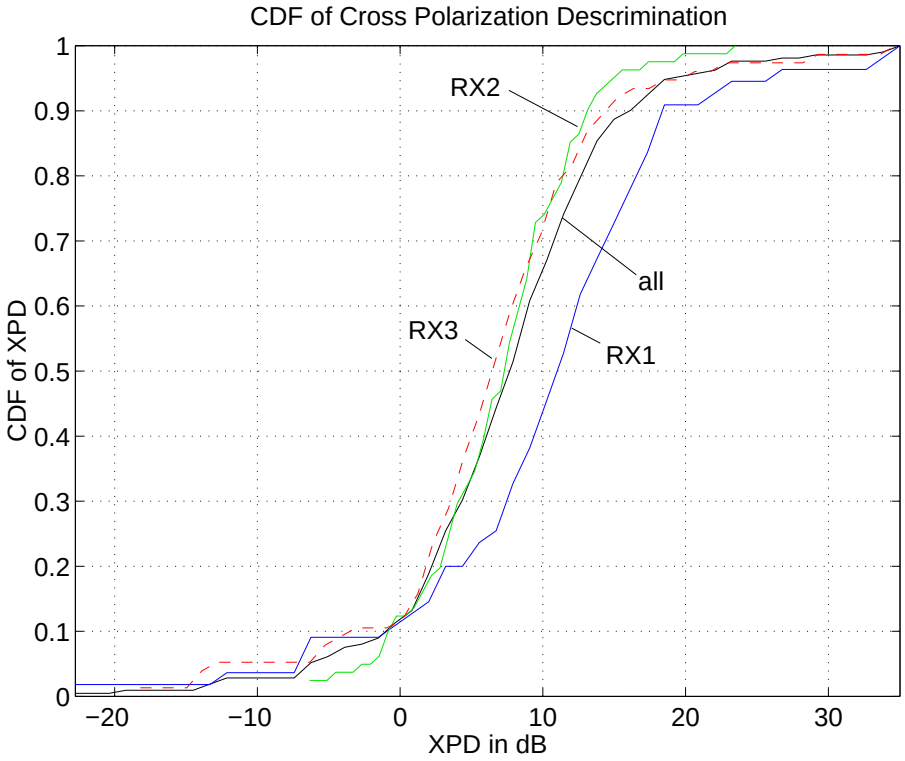

Fig. 20. CDF of Cross Polarization Discrimination of all TX positions